Disruption of quantum oscillations by an incommensurate charge density wave

Yi Zhang, Akash V. Maharaj, and Steven Kivelson

Phys. Rev. B **91**, 085105 — Published 9 February 2015

DOI: 10.1103/PhysRevB.91.085105

Disruption of quantum oscillations by an incommensurate charge density wave

Yi Zhang, Akash V. Maharaj, and Steven Kivelson
Department of Physics, Stanford University, Stanford, California 94305, USA
(Dated: January 26, 2015)

Because a material with an incommensurate charge density wave (ICDW) is only quasi-periodic, Bloch's theorem does not apply and there is no sharply defined Fermi surface. We will show that, as a consequence, there are no quantum oscillations which are truly periodic functions of $1/B$ (where B is the magnitude of an applied magnetic field). For a weak ICDW, there exist broad ranges of $1/B$ in which approximately periodic variations occur, but with frequencies that vary inexorably in an unending cascade with increasing $1/B$. For a strong ICDW, e.g. in a quasi-crystal, no quantum oscillations survive at all. Rational and irrational numbers really are different.

I. INTRODUCTION

Quantum oscillations (QOs) provide powerful experimental avenues to precisely characterize the Fermi surface structure in an electron system[1,2]. At zero temperature and in the limit of small magnetic field B (where the semiclassical approximation is asymptotically exact), measurable quantities such as the density of states (DOS) and various transport properties oscillate as a function of $1/B$ with a periodicity that is inversely proportional to the cross-sectional area of the Fermi surface. In the presence of a commensurate charge density wave (CDW), the QOs can be simply understood by folding the momentum space Brillouin zone in accord with the enlargement of the crystal unit cell. In the case of an incommensurate charge density wave(ICDW), however, the translational symmetry along the direction of the CDW wave vector (or vectors) is completely broken; Bloch's theorem no longer applies, and hence the notion of a Fermi surface is at best an approximate concept. Nonetheless, it has been widely accepted that new oscillation periods arise from the reconstructed electron and hole pockets that result from the perturbative folding of the Fermi surface in a manner similar to that of the commensurate case[3–5].

We have extensively studied the problem of QOs in a two-dimensional system in the presence of a unidirectional ICDW. We obtain numerical solutions on systems with a linear dimension up to $\sim O\left(10^6\right)$ sites using an efficient recursive Green's function method. For weak ICDW potentials $V \ll W$ where W is the bandwidth, we obtain a perturbative understanding of these results, while larger values of V/W can be understood by introducing an exact duality between the two-dimensional system with a unidirectional ICDW, and a three-dimensional system without the ICDW but with an additional magnetic flux. For the two-dimensional system with an ICDW of ordering vector Q and amplitude V, the dual three-dimensional system has a hopping matrix element $V/2$ in the out-of-plane ($\hat{z}$) direction, and a "tilted" magnetic field $\vec{B}^{eff} = B\hat{z} + (Q/2\pi)\hat{y}$ where $\hat{x}$ and $\hat{y}$ are the in-plane directions parallel and perpendicular to the charge ordering vector (where magnetic fields are measured in units of a flux quanta per unit cell). This mapping is readily generalized to other dimensions, as well as to the case of bidirectional ICDW order.

We find that there is no limit in which perfectly periodic QOs occur in the presence of an ICDW. In the strong coupling limit, for V/W greater than a critical value of order 1, there are no well defined QOs at all. In the dual system, the critical V/W is identified with the point at which the underlying three-dimensional Fermi surface transforms from a quasi-two-dimensional cylinder to a closed three-dimensional surface. This limit likely applies to the case of quasi-crystals in which the incommensurate potential is not small in any sense. By contrast, in the small V/W limit, oscillations that approximate the QOs of a true crystal are observed over large but finite intervals of $1/B$, but the observed period varies depending on the range of B studied.

The nature of the QOs for small V/W, and the manner in which they deviate from strict periodicity can be understood intuitively in terms of the conventional theory of magnetic breakdown as a perturbative effect. Specifically, there is a hierarchy of gaps on the Fermi surface, $\Delta_n \sim W(V/W)^n$, whose magnitudes are governed by the lowest order in perturbation theory at which they appear. Depending on the position of the unperturbed Fermi surface and its relation to the CDW ordering vector, only some of these gaps open on the Fermi surface, and so it is only these that matter. The hierarchy of gaps on the Fermi surface terminates at $n_{\max} \leq q$ for a q^{th} order commensurate CDW, but it continues to arbitrarily high n in the incommensurate case. In a given range of B, magnetic breakdown effectively eliminates the effect on the electron dynamics of all gaps that are sufficiently small that $\Delta^2/W \ll \omega_c$, where $\omega_c \sim WB$ is the effective cyclotron energy, while all gaps that are large compared to $\sqrt{\omega_c W}$ are respected by the semiclassical dynamics. If $n = N$ and $n = N + M$ are two sequential terms in this hierarchy, then for small V/W there exists a parametrically broad range of fields, $(\Delta_N/W)^2 \gg B \gg (\Delta_{N+M}/W)^2$, in which all gaps of order $n \geq N + M$ can be neglected, but the Fermi surface is effectively reconstructed by all gaps with $n \leq N$. However, inevitably, a further reconstruction of the Fermi surface must occur in some order of perturbation theory, giving a fractal character to the QO spectrum.

The rest of this paper is organized as follows. Sec. II reviews the canonical understanding of QOs in the presence and absence of CDWs. In Sec. III we introduce the tight binding model which forms the basis of our numerical analysis, and also discuss its duality properties. Numerical results are presented in Sec. IV, where we show the field dependence of QO periods for a commensurate CDW and a small amplitude ICDW, along with the spectacular absence of QOs for a large

amplitude ICDW. We also explain the eventual breakdown of the perturbative picture for the ICDW QOs. In Sec. V we numerically verify the exactness of the duality picture, using this view to uncover several novel properties of ICDW in magnetic fields. Finally, Sec. VI discusses further applications of this model to localization problems in one dimension as well as the case of bidirectional ICDW order.

II. CHARGE DENSITY WAVES IN A MAGNETIC FIELD

A. Quantum oscillations in ordinary metals

Quantum oscillatory phenomena can be generally understood to arise from the semi-classical quantization of electronic energies in an applied magnetic field – which is asymptotically exact in the $B \to 0$ limit. The dynamics of Bloch electrons in an applied magnetic field is given semi-classically by the Lorentz force law:

$$\hbar \frac{d\vec{k}}{dt} = -e\left[\vec{v}(\vec{k}) \times \vec{B}\right] = \frac{e}{\hbar}\left(\vec{B} \times \frac{dE(\vec{k})}{d\vec{k}}\right), \tag{1}$$

where $\vec{v}(\vec{k}) = (1/\hbar)\, dE/d\vec{k}$ is the electron group velocity. This implies $\vec{k} \cdot \vec{B} = 0$ and $dE(\vec{k})/dt = 0$, i.e. the electrons move in orbits of constant energy in planes perpendicular to the magnetic field.

In the absence of any Berry phase, the quantum phase the electrons accrue on each orbit around the Fermi surface is $\hbar S_k/eB$, where S_k is the area of Fermi surface cross section perpendicular to the applied magnetic field. Thus the maximum and minimum values of S_k govern the interference between multiple trajectories. Maxima in the semiclassical DOS (corresponding to the point at which a Landau level just crosses the Fermi energy) occur whenever

$$\frac{1}{B} = \left(n + \frac{1}{2}\right)\frac{4\pi^2}{\Phi_0 S_k} \tag{2}$$

for integer $n \in \mathbb{Z}$ where $\Phi_0 = h/e$ is the magnetic flux quantum. For fixed Fermi energy (and hence constant S_k) this leads to perfectly periodic QOs with period $\Delta(1/B) = 2\pi e/\hbar S_k$.

B. Commensurate CDWs and magnetic breakdown

The above arguments can be straightforwardly applied to systems in which the translation symmetry of the crystal is spontaneously broken by a commensurate CDW with wavevector $\vec{Q} = Q\hat{x}$ where, in units in which the lattice constant is $a = 1$, $Q = 2\pi p/q$ with $p, q \in \mathbb{Z}$ relatively prime. This simply defines a new crystal structure with q times as large a unit cell and q times as many bands in a folded Brillouin zone which is q times smaller in the $\hat{x}$ direction. Generically,[12–14] the CDW causes a "reconstruction" of the Fermi surface due to gaps that open at the new Brillouin zone-boundary, resulting in smaller electron and hole pockets (plus open Fermi surfaces that do not contribute to the QOs), thus giving rise to new periodicities in the QOs. The reconstruction can be viewed as arising from processes in which the electrons on the Fermi surface are scattered by the CDW with momentum transfer $\pm nQ\hat{x}$ modulo $2\pi\hat{x}$. In the case of a weak sinusoidal density wave, $V/W \ll 1$, there is a hierarchy of scales associated with these processes depending on n, as such processes arise first in n^{th} order perturbation theory, see Fig. 1.

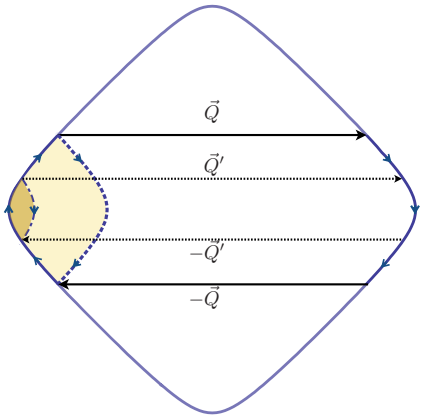

FIG. 1. The Fermi surface reconstruction with a momentum transfer of $\pm Q$ by scattering from a CDW is shown as the yellow-colored region (both the dark and light yellow regions). In addition, a higher order scattering with a momentum transfer of $\pm Q'$ may lead to a smaller pocket (dark yellow region) and so on. Consequently, there may be a hierarchy of Fermi surface pockets protected by gaps of different sizes.

In the notation used in the introduction, gaps indexed in this way depend parametrically on V as $\Delta_n = \alpha W (V/W)^n \left[1 + O(V/W)^2\right]$ where α does not depend on V. Depending on the relation between the Fermi surface location and the ordering vector Q, gaps with a given index n may not involve states at the Fermi surface, in which case they can be neglected for present purposes. For instance, if Q' in Fig. 1 were slightly longer, it would fail to span the indicated Fermi surface, and so would not produce any Fermi surface reconstruction. Notice that the area of the reconstructed Fermi surface pockets is purely geometric in the limit of vanishingly small V/W, determined solely by the structure of the underlying Fermi surface and the specified CDW ordering vector, but for finite V the opening of gaps causes a non-zero displacement of the Fermi surface which can produce changes in the area of the various pockets of order Δ_n/W. This effect becomes qualitatively significant if V/W is not small, in which case the perturbative approach must be abandoned.

For finite field strength B corrections to semiclassical quantization arise due to 'magnetic breakdown', associated with transitions between semiclassical trajectories. It is easy to show[6–8] that magnetic breakdown is negligible so long as $\ell \delta k \gg 1$, where $\ell = \sqrt{\Phi_0/2\pi B}$ is the magnetic length and δk is the distance of closest approach in reciprocal space between two semi-classical trajectories. (The precise criterion depends on the local curvature of the trajectories as well[8,9].)

Alternatively, for weak CDW order, this criterion can be expressed as $\omega_c \ll \Delta^2/W$, where ω_c is the cyclotron energy and Δ is the relevant gap induced by the CDW. When there exists a series of Fermi surface pockets produced by gaps of different sizes from multiple orders of reconstructions, this results in a corresponding hierarchy of breakdown magnetic fields.

C. Incommensurate CDW in a magnetic field

When the period of charge modulation is not a rational multiple of the underlying lattice spacing, *i.e.* when $Q = 2\pi\alpha$ where α is an irrational number, the CDW is referred to as incommensurate. While many properties of ICDW materials can be understood by treating the CDW potential perturbatively, or better still by approximating α by a nearby commensurate approximant, $p/q \approx \alpha$, we will show in this paper that an exact treatment of the problem reveals a number of fundamental properties that are not captured by this type of approximation.

III. THE MODEL

To begin with, we define a general model on a d-dimensional hyper-cubic lattice in the presence of a uniform magnetic field and a CDW potential:

$$H = -\sum_{\langle\vec{r},\vec{r}'\rangle}\left[t_{\vec{r}-\vec{r}'}\exp\left[iA(\vec{r},\vec{r}')\right]c^\dagger_{\vec{r}}c_{\vec{r}'} + \text{h.c.}\right] - \sum_{\vec{r}} U(\vec{r})c^\dagger_{\vec{r}}c_{\vec{r}} \quad (3)$$

where $c^\dagger_{\vec{r}}$ creates an electron on site $\vec{r}$, $\langle\vec{r},\vec{r}'\rangle$ designates nearest-neighbor sites, $t_\nu \equiv t(\pm\hat{e}_\nu)$ is assumed real and positive, but can depend on direction $\hat{e}_\nu$ with ν running from 1 to d (with the convention $\hat{e}_1 = \hat{x}$, $\hat{e}_2 = \hat{y}$, etc.), the magnetic flux through any plaquette in units in which the flux quantum is $\Phi_0 = 2\pi$ is given by the sum of A around the plaquette, and by definition $A(\vec{r},\vec{r}') = -A(\vec{r}',\vec{r})$. In all cases, we will assume the flux is spatially uniform and penetrates only plaquettes that are parallel to $\hat{x}$. We are thus free to chose a gauge that preserves translational symmetry in all but the $\hat{x}$ direction, $A(\vec{r},\vec{r}+\hat{e}_\nu) = \Phi_\nu\,\vec{r}\cdot\hat{x} = \Phi_\nu\,x$, where, for example, $\Phi_2 \equiv \Phi_y = \Phi$ is the flux through each plaquette in the $x-y$ plane, and $\Phi_1 \equiv \Phi_x = 0$. For the present, we will also consider a unidirectional CDW in the $\hat{x}$ direction which consists of a small number m of distinct Fourier components,

$$U(\vec{r}) = \sum_{j=1}^{m} V_j\cos[Q_j x - \theta_j]. \quad (4)$$

Here θ_j is the relative phase between a given component of the CDW and the underlying lattice, and $x_j \equiv \theta_j/Q_j$ can be interpreted as the location of the minimum of the corresponding CDW potential in Eq. 3 in continuum space.

Because the CDW is unidirectional and we have chosen the appropriate gauge, we can exploit translation invariance to Bloch diagonalize the Hamiltonian by Fourier transform perpendicular to $\hat{x}$. We define

$$a_{x,\vec{k}} \equiv (N_\perp)^{-d/2}\sum_{\vec{r}_\perp} e^{i\vec{k}\cdot\vec{r}_\perp}c_{\vec{r}_\perp+x\hat{x}} \quad (5)$$

where $\vec{r}_\perp \equiv \vec{r} - x\hat{x}$ and $\vec{k}$ is the corresponding $d-1$ dimensional Bloch vector. In terms of these, $H = \sum_{\vec{k}} H_{\vec{k}}$ with

$$H_{\vec{k}} = -\sum_x t_x\left(a^\dagger_{x,\vec{k}}a_{x+1,\vec{k}} + \text{h.c.}\right) + \left[2\sum_{\nu=2}^{d} t_\nu\cos(\Phi_\nu x - k_\nu) + \sum_{j=1}^{m} V_j\cos(Q_j x - \theta_j)\right]a^\dagger_{x,\vec{k}}a_{x,\vec{k}} \quad (6)$$

Thus, for given $\vec{k}$, the generic problem is equivalent to a problem in one dimension. Moreover, it is immediately apparent from Eq. 6 that there is a formal equivalence between higher dimensional problems with a magnetic field and lower dimensional problems with more components of the CDW; e.g. with all $V_j = 0$ there is the familiar relationship between the Hofstadter problem of a two-dimensional crystal in the presence of a uniform flux Φ per plaquette and the corresponding one-dimensional problem (governed by Harper's or the "almost Mathieu" equation[10,11]) of a particle in a sinusoidal potential.[17]

Duality relations: The problem of present interest is that of the two-dimensional crystal subjected to a uniform flux Φ and a unidirectional CDW potential $V\cos[Qx-\theta]$. We now see that this is equivalent both to a one-dimensional system with the doubly periodic potential, $U(\vec{r}) = V\cos[Qx-\theta] + 2t_y\cos[\Phi x - k_y]$, and the anisotropic three-dimensional crystal with hopping matrix elements t_x, t_y and $t_z = V/2$ in, respectively, the $\hat{x}$, $\hat{y}$, and $\hat{z}$ directions subjected to a uniform magnetic field with flux Φ through each xy plaquette and flux Q through each xz plaquette (see Fig. 2). We will use the one-dimensional representation of the problem as the basis of our numerical study. However, we gain physical insight into the solution and approximate analytic understanding by viewing it as a translationally invariant (crystalline) three-dimensional problem in a tilted magnetic field. We also note that higher harmonic components of the CDW potential with wave vectors nQ, $n \in \mathbb{Z}$, correspond to the same net magnetic field but further neighbor hoppings in the $\hat{z}$ direction thus more generic k_z dispersions.

There is still the issue of the sum over $\vec{k}$. However, for the one-dimensional problem with a multi-component ICDW potential for which Q_i/Q_j is irrational for all $i \neq j$, it is easy to see and straightforward to prove that *in the thermodynamic limit*, the spectrum is independent of the the phases θ_j, that is to say that there is a sliding symmetry for each component of the CDW. Translated to the magnetic flux problem, since Φ_ν is generically an irrational multiple of Φ_0, this implies that (except in fine tuned circumstances), the spectrum of Eq. 6 will be independent of $\vec{k}$. Thus, for all thermodynamic quantities, the sum over $\vec{k}$ simply produces a degeneracy factor of $N_\perp$ for each eigenstate.

Notation and Units: We will henceforth suppress the index $\vec{k}$ on all quantities, (*e.g.* $a_{x,\vec{k}}$ will be represented as a_x). We

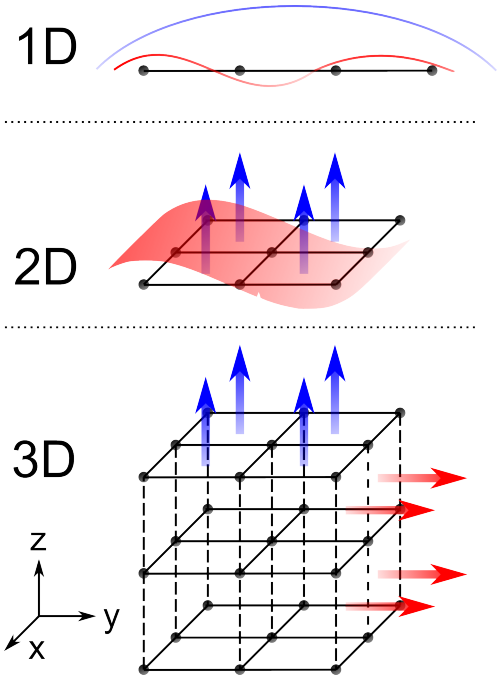

FIG. 2. Upper panel: A one-dimensional model with two incommensurately periodic potentials, one with amplitude 2 and wave vector Φ (blue curve) and the other with amplitude V and wave vector Q (red curve). Middle panel: The equivalent two-dimensional square lattice model with an ICDW (red curve) and a magnetic flux (blue arrow) $\Phi = 2\pi B$ per plaquette. Lower panel: The effective cubic lattice model in three dimensions. Here the hopping amplitudes are 1 along the $\hat{x}$ and $\hat{y}$ directions (solid lines), and $V/2$ along the $\hat{z}$ direction (dashed lines), and an additional magnetic flux of Q is now present through the xz plaquettes (the red arrow).

will specialize to the case in which the two-dimensional band structure is isotropic, $t_x = t_y = t$, and will use units of energy such that $t = 1$. Recall that we have adopted units of length such that the lattice constant is 1, and units of magnetic field $B = \Phi/2\pi$ such that $\Phi_0 = 2\pi$.

IV. RESULTS OF NUMERICAL EXPERIMENTS

In our numerical studies, we compute two physical quantities which are related to the Green's function for the doubly incommensurate one-dimensional problem with open boundary conditions, Eq. 6 with $d = 2$ and $n = 1$. The Green's function for each k_y is defined as the matrix inverse:

$$G_{k_y}(x, x') = \left(\mu + i\delta - H_{k_y}\right)^{-1}_{x,x'} \tag{7}$$

where μ is the chemical potential and $i\delta$ is a very small imaginary part to round off the singularities, which for large systems can always be chosen so that, to any desired accuracy, the results are δ independent. We calculate both the DOS ρ at the Fermi level

$$\rho_{k_y}(\mu) = -\frac{1}{\pi L}\sum_x \mathrm{Im} G_{k_y}(x, x) \tag{8}$$

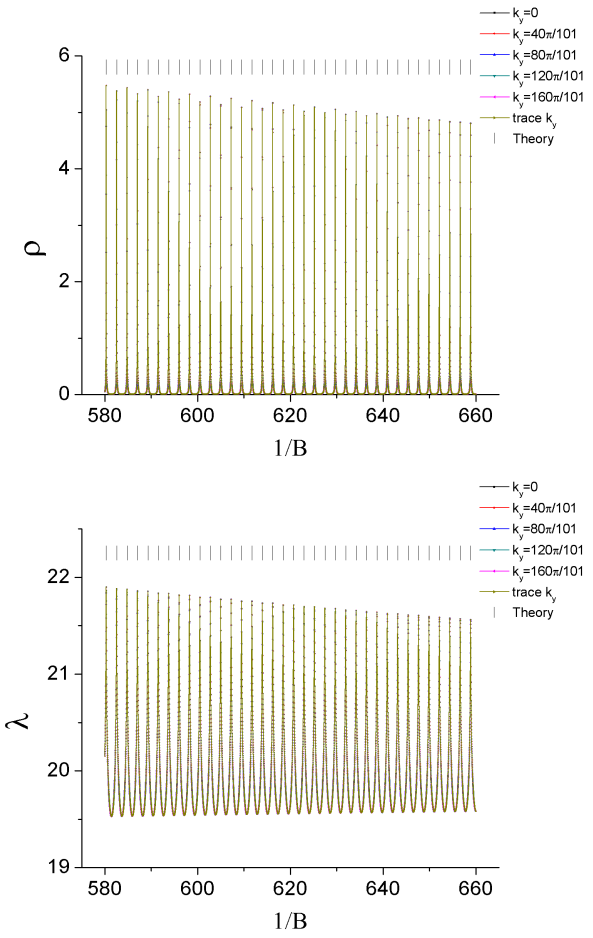

FIG. 3. (Upper panel) the DOS ρ and (lower panel) the localization length λ versus $1/B$ calculated from various values of k_y as well by as tracing/averaging over all k_y (taking $L_y = 101$) for a system of length $L = 10^5$ without a CDW ($V = 0$). For comparison, the marks at the top of each figure are the theoretical values of interference maxima based on the Fermi surface area of $S_k = 0.44546 S_{BZ}$.

and the localization length λ that defines the exponential decay of the Green's function $G_{k_y}(1, L) \sim \exp(-L/\lambda_{k_y})$ between two ends of the system. Further details on our numerical methods are presented in the Appendix A.

A. Results for a commensurate CDW

We first benchmark our methods on the same model with no CDW ($V = 0$) or a commensurate CDW ($Q = \pi$, $V = 0.16$). We set the chemical potential $\mu = -0.2$, corresponding to slight hole doping away from half filling to avoid complications that arise from (fine-tuned) Fermi surface nesting on a bipartite lattice when $\mu = 0$; our conclusions are readily generalizable to other chemical potentials and shapes of the Fermi surface.

To study the QOs for $V = 0$, we extract the localization length λ and DOS ρ over a range of magnetic field on a $L = 10^5$ system. As shown in Fig. 3, both the DOS ρ (up-

per panel) and the localization length λ (lower panel) exhibit a clear single-period oscillation. By linearly fitting the locations of the peaks we obtain the period $\Delta(1/B) = 2.2452$, which corresponds to a momentum space area:

$$S_k = \frac{4\pi^2}{\Delta(1/B)} = 0.4454 S_{BZ} \tag{9}$$

where $S_{BZ} = (2\pi)^2$ is the area of the entire Brillouin zone of the square lattice. For comparison, given the zero-field dispersion relation of Eq. 3 with the assumed value of the chemical potential, the Fermi surface enclosed area in the absence of any CDW is $S_k = 0.44546 S_{BZ}$. To highlight the high accuracy of our results, we have also marked the theoretically expected locations of the maxima from Eq. 2 at the top of each figure.

We have checked the expected k_y independence of the results by repeating the calculation for different choices of k_y as well as by averaging over k_y as shown in Fig. 3. Henceforth we suppress the k_y label for both ρ and λ.

As another benchmark, we have studied QOs in the presence of a commensurate CDW: $V = 0.16$ and $Q = \pi$ for $L = 2\times10^5$; the results for the DOS and the localization length are shown in the upper and middle panels of Fig. 4, respectively. A Fourier transform (Fig. 4 insets) reveals peaks and higher harmonics[18] that correspond to a fundamental period of $\Delta(1/B) = 10.464$. This, in turn, reflects a momentum space area $S_k = 0.1911 S_{BZ'}$, where $S_{BZ'} = S_{BZ}/2$ is the area of the folded Brillouin zone according to the enlarged unit cell. For the given parameters, the Fermi surface consists of only one closed pocket with an enclosed area of $S_k = 0.1909 S_{BZ'}$.

Strictly speaking, at any finite magnetic field, the QO periods are magnetic-field dependent due to corrections to the semiclassical results associated with magnetic breakdown. This behavior is illustrated in the lower panel of Fig. 4, which is the same model but with larger values of B ($1/B \in [120, 160]$). QOs with a period $\Delta(1/B) = 2.245$ are clearly seen, which corresponds to the Fermi surface area in the absence of the CDW potential ($V = 0$). While oscillations with a period corresponding to the reconstructed Fermi surface, $\Delta(1/B) = 10.463$, are also vaguely discernible in this field range; they become dominant only at smaller fields.

B. Results for an ICDW

We now consider systems with ICDW, and discuss the consequences within various regimes of magnetic field strength and CDW amplitude.

1. *Reconstructed Fermi-surface in the perturbative regime*

Many studies[3–5] of QOs in an ICDW use perturbative arguments to evaluate the reconstructed Fermi surfaces. As indicated before, this approach is partially justified in the limit of weak CDW potentials $V \ll t$, where the result can be visualized dynamically as electrons precessing in semiclassical orbits around a closed Fermi surface, and only occasionally

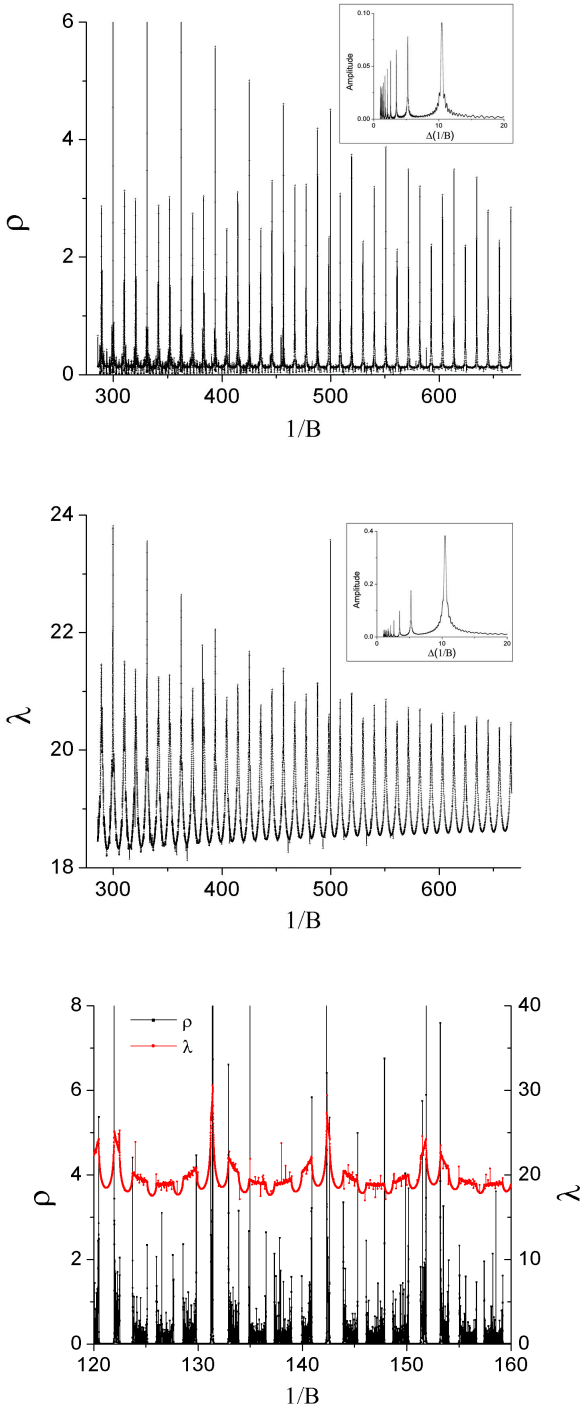

FIG. 4. The DOS ρ (upper panel) and the localization length (middle panel) versus the inverse magnetic field $1/B$ for a system of length $L = 2\times10^5$ with parameters $\mu = -0.2$, $V = 0.16$ and $Q = \pi$. Insets: the Fourier transform of the QOs exhibits a clear peak at period $\Delta(1/B) = 10.464$ corresponding to the fundamental period. Lower panel: the QOs behavior of the DOS and the localization length over a range of larger magnetic fields B.

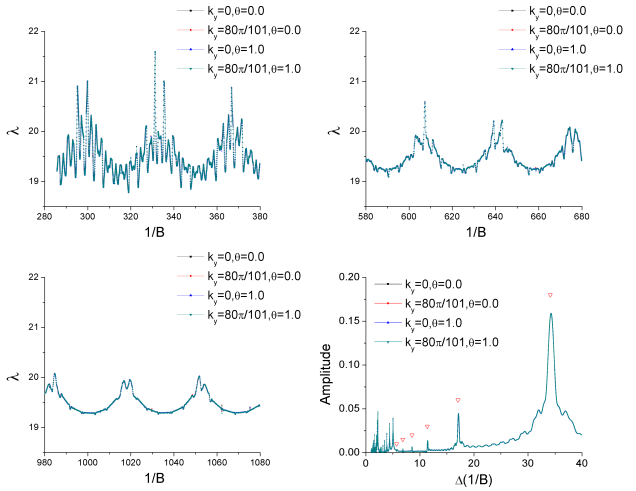

FIG. 5. The localization length λ versus the inverse magnetic field $1/B$ for a system of length $L = 7.2 \times 10^6$, $\mu = -0.2$ and an ICDW with $Q = 2.0$ and $V = 0.16$ over various ranges of the magnetic field. The last figure is the Fourier transform of the QOs for the range $1/B \in [280, 1400]$. The red triangles mark the anticipated period and corresponding higher harmonics from lowest order perturbation theory. Different choices of k_y and θ are shown in different colors and their results clearly collapse onto the same curve.

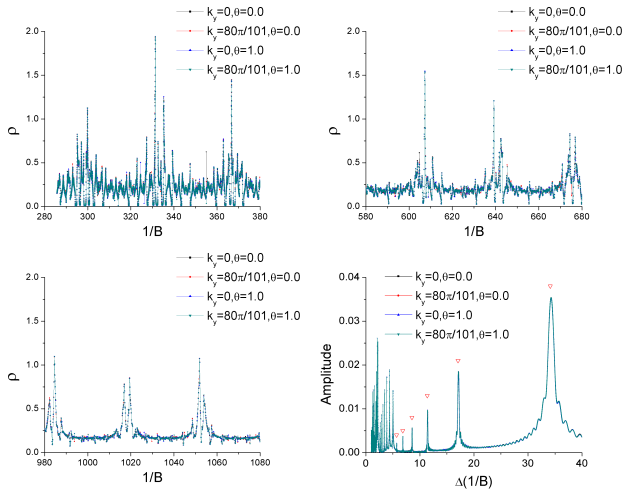

FIG. 6. The DOS ρ versus the inverse magnetic field $1/B$ for a system of length $L = 4 \times 10^6$, $\mu = -0.2$ and an ICDW with $Q = 2.0$ and $V = 0.16$ over various ranges of the magnetic field. The last figure is the Fourier transform of the QOs for the range $1/B \in [280, 1400]$. The red triangles mark the anticipated period and corresponding higher harmonics from lowest order perturbation theory. Different choices of k_y and θ are shown in different colors; the results clearly collapse onto the same curve.

picking up momentum $\pm Q$ to jump from one section of the Fermi surface to another.

To have a secure basis for our discussion, we begin by applying the same numerical technique described above to the incommensurate case. As far as we are aware of, this is the first numerical solution of the fully incommensurate prob-

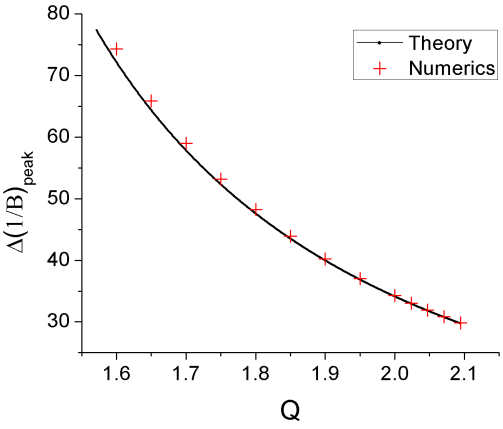

FIG. 7. Red crosses: The calculated QOs characteristic periods versus the ICDW wave vector Q with $V = 0.16$, $\mu = -0.2$ and $L = 2 \times 10^5$. The black solid curve is the theoretical values derived from the area of the first-order reconstructed Fermi surfaces.

lem. To begin with, we consider a CDW with wave vector $Q = 2 = 2\pi(1/\pi)$ and potential $V = 0.16$ with $\mu = -0.2$; the results are shown in Fig. 5 (localization length λ) and Fig. 6 (DOS ρ). For better convergence and accuracy we work with systems of size $L = 7.2 \times 10^6$ for the localization length and $L = 4{\times}10^6$ for the DOS calculations. We find QOs with period corresponding to the original (unreconstructed) Fermi surface $\Delta(1/B) = 2.245$ which are dominant when the field is not too small, while another with $\Delta(1/B) = 34.271$ becomes increasingly prominent at lower fields; each of these fundamentals is accompanied by a complicated spectrum of higher harmonics. In lowest order perturbation theory with a momentum transfer of $\pm Q$, the area enclosed by the reconstructed Fermi pocket (illustrated schematically as the light yellow patch in Fig. 1) is $S_k = 2.931\% S_{BZ}$ of the original Brillouin zone, which corresponds to a period of $\Delta(1/B) = 34.12$ as we have marked in Fig. 5 and 6 together with corresponding higher harmonics.

As expected, the above results are independent of the specific choices of k_y and θ.

To further test the perturbative approach, we repeated the above calculations with a series of ICDWs with wave vectors in the range $Q \in (2\pi/4, 2\pi/3)$ and with fixed values of V and μ. The main oscillation periods obtained from the peak locations in the Fourier transformed spectra are indicated by the crosses in Fig. 7. For comparison, we also include the theoretical QO period corresponding to the pocket sizes predicted from the lowest order perturbation. The consistency is remarkable.

2. *Breakdown of perturbation theory as $B \to 0$*

We have anticipated that the finite-order perturbative results inevitably break down for small enough magnetic fields. Since any gaps generated in n^{th} order perturbation theory are of order $W(V/W)^n$, the characteristic magnetic field scale above

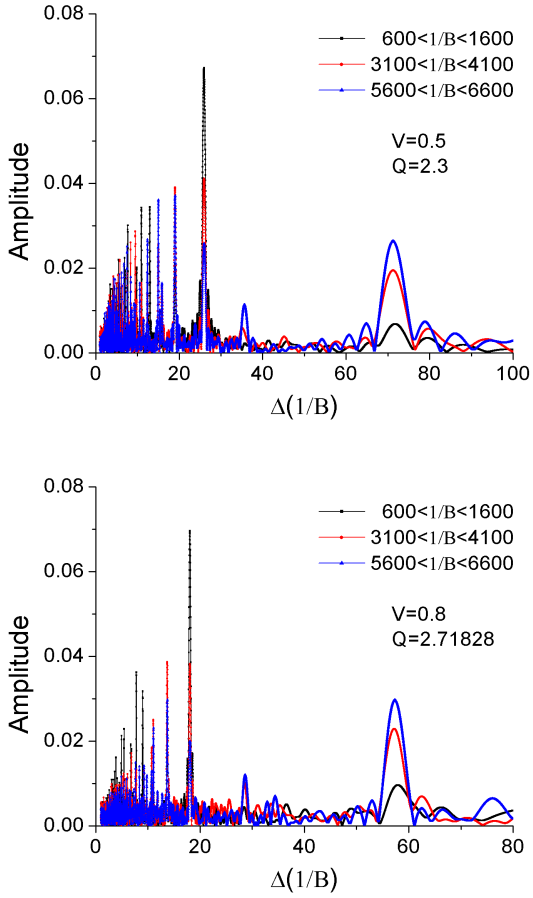

FIG. 8. The Fourier transformations of the QOs of the DOS ρ with parameters $V = 0.5$, $Q = 2.3$, $\mu = -0.2$ (upper panel) and $V = 0.8$, $Q = 2.71828$, $\mu = -0.2$ (lower panel) over various ranges of the magnetic field. The system size is $L = 2 \times 10^5$.

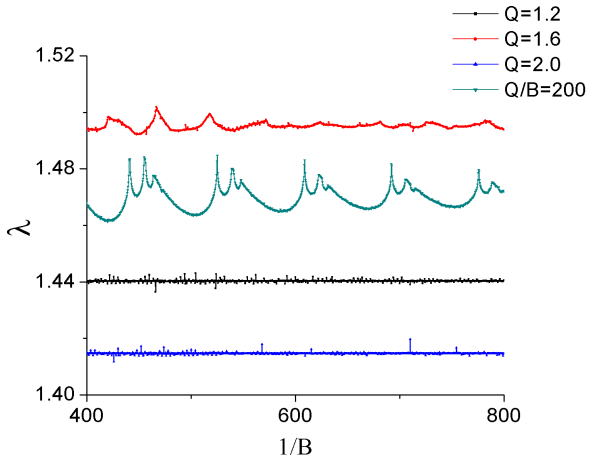

FIG. 9. The localization length λ in the presence of a strong ICDW $V = 1.6$, $\mu = -2.5$ and $Q = 1.2$ (black), $Q = 1.6$ (red) and $Q = 2.0$ (blue). For comparison, we include the QOs of localization length λ with $V = 1.6$, $\mu = -2.5$ and $Q/B = 200$ for the same range of magnetic field B (green) with $L = 7.2 \times 10^5$.

which these gaps are eliminated by magnetic breakdown is expected to scale with V according to $B_n \sim V^{2n}$. This leads to the cascade of field ranges that has already been exhibited in the commensurate case above. The difference is that, while in the case of commensurability q no new gaps are generated beyond q^{th} order perturbation theory, in the incommensurate case no termination of the cascade is expected. For numerical experiments, it is simpler to study this working in a fixed range of magnetic fields and increasing the magnitude of the CDW potential V, rather than by going to still lower fields.

We thus calculate the QOs of the DOS for somewhat larger magnitude of the CDW potential. The results for two illustrative examples: $Q = 2.3$, $V = 0.5$ and $Q = 2.71828$, $V = 0.8$ are shown in Fig. 8. We have kept the chemical potential $\mu = -0.2$ and taken $L = 2 \times 10^5$ in these calculations. Different ranges of the magnetic field are shown in different colors to emphasize the cross-over between different regimes.

For $Q = 2.3$, distinct points on the Fermi surface are connected by Q and $2Q$, so we expect the QOs to be determined principally by the area of the unperturbed Fermi surface for high fields, $B > B_1 \sim (V/W)^2$, the 1st order perturbatively reconstructed Fermi surface for $B_1 > B > B_2 \sim (V/W)^4$, and the 2nd order reconstructed Fermi surface for $B_2 > B > B_3 \sim (V/W)^6$. We do not report the data for the highest fields, $B > B_1$ but in the upper panel of Fig. 8 one can observe a crossover from the dominant oscillations having period of $\Delta(1/B) = 25.97$ in the higher field range to $\Delta(1/B) = 71.24$ in the lower; these are consistent with the expected frequencies corresponding to a Fermi surface reconstructed to first and second order in V, respectively. On the other hand, for $Q = 2.71828$, the scattering vector $2Q$ does not span the Fermi surface, so no new gaps on the Fermi surface are opened in second order in perturbation theory. However, scattering with momentum Q and $3Q$ (modulo 2π) opens distinct gaps on the Fermi surface, and indeed the expected crossover from a dominant oscillation period of $\Delta(1/B) = 18.07$ at relatively high fields to $\Delta(1/B) = 57.32$ at somewhat lower fields is observed, in good agreement with the expected periods from the perturbative construction.

We conclude from the numerical results for V smaller than W and not too small magnetic fields that perturbation theory provides a grossly satisfactory description of the structure of the QOs, and that it also provides a vivid account of the manner in which the perturbative results to any given order break down for low enough magnetic fields.

3. *Absence of all QOs for large V*

For large $V > W$, clearly perturbation theory is expected to have no regime of validity. On the other hand, the behavior can be well understood in a dual picture using the mapping of the problem onto the properties of a three-dimensional crystal with no CDW but in the presence of a tilted effective magnetic field, $\vec{B}^{\,\mathrm{eff}} = [B\hat{z} + Q\hat{y}/2\pi]$, as we will discuss in Sec. V. In particular, we will show that for V larger than a characteristic

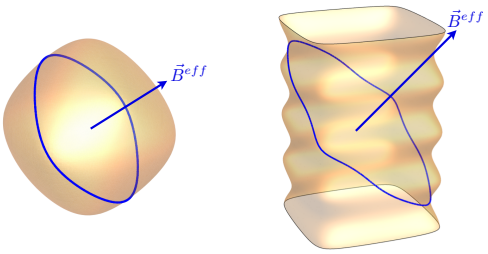

FIG. 10. Zero-field Fermi surfaces of the three-dimensional effective theory for (left) a strong ICDW with $V = 1.6$, $\mu = -2.5$ and (right) a weak ICDW with $V = 0.16$, $\mu = -0.2$. The cross sections perpendicular to $\vec{B}^{\,\mathrm{eff}}$ are shown as the blue lines.

magnitude V_c (defined as the point at which a Lifshitz transition occurs in the band-structure of the dual three-dimensional crystal), there are no well defined QOs at all!

To illustrate the basic phenomenology, we show in Fig. 9 the localization length as a function of B in the presence of a reasonably strong CDW potential with $V = 1.6$, $\mu = -2.5$ and $Q = 1.2$, 1.6, and 2.0. Also shown in the figure is the corresponding curve in the unphysical case in which the CDW ordering vector varies in proportion to the magnetic field as $Q = \alpha B$, with the constant $\alpha = 200$ chosen so that Q is of order 1 in the range of fields represented in the figure. Manifestly, the three curves with fixed Q show no periodic oscillations at all, and indeed relatively weak magnetic field dependence of any sort. However, when we vary Q in proportion to B we do see perfectly periodic QOs, albeit with a rather unusual harmonic content. These features are easily understood in the dual three-dimensional picture, which we now discuss.

V. THE DUAL THREE-DIMENSIONAL VIEW OF QUANTUM OSCILLATIONS

The advantage of the dual three-dimensional representation of the problem is that it allows us to treat the CDW potential V non-perturbatively, by incorporating it into the band-structure. Then provided the magnitude of $\vec{B}^{\,\mathrm{eff}} = (B\hat{z} + Q\hat{y}/2\pi)$ is sufficiently small (in a sense we will define below) we can again treat the electron dynamics semiclassically, although now on a three-dimensional Fermi surface.

A. Numerical tests of duality

Although the duality is exact in the thermodynamic limit, we begin by performing numerical tests to establish the accuracy of the approach for the system sizes used in this study. For this purpose, we use the same numerical approach to solve the one-dimensional problem with a doubly incommensurate potential, and compare the results to expectations based on the three-dimensional effective theory. This is made simpler if we consider the unphysical situation in which both B and Q are varied simultaneously, while keeping the ratio B/Q fixed, so that the direction of the effective magnetic field $\vec{B}^{\,\mathrm{eff}} = (B\hat{z} + Q\hat{y}/2\pi)$ remains fixed. Semiclassically, QO frequencies are simply given by the maximum and minimum cross-section areas of the three-dimensional Fermi surface perpendicular to $\vec{B}^{\,\mathrm{eff}}$, and the numerical results in Fig. 9 confirm QOs are present, even for large V.

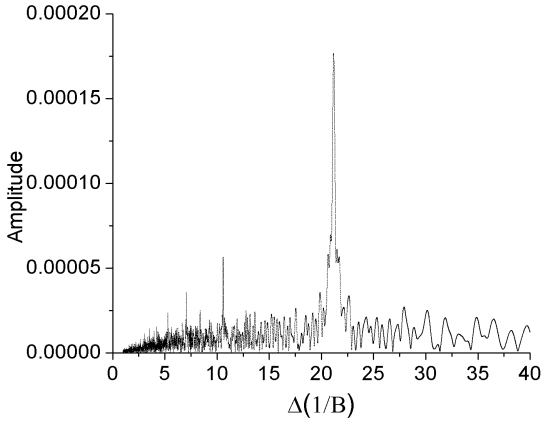

FIG. 11. Fourier transformations of the QOs of the DOS ρ with a strong ICDW $V = 1.6$ and $\mu = -2.5$ and $Q/B = 50$ over a range of $1/B \in [500, 2500]$. A clear peak is observed at $\Delta(1/B) = 21.175$ as well as its higher harmonics. The system size is $L = 7.2 \times 10^5$.

Strong CDW ($V = 1.6$, $\mu = -2.5$): In this case, the CDW potential is sufficiently large that the Fermi surface in the three-dimensional effective theory is closed. Fig. 10 (left panel) provides an illustration of the three-dimensional Fermi surface structure, which is topologically equivalent to a sphere and closed in the $\hat{z}$ direction. We numerically obtain QOs of the DOS for $Q/B = 50$ over a range of $1/B \in [500, 2500]$ on system size of length $L = 7.2 \times 10^5$, and the resulting Fourier transforms is shown in Fig. 11. A clear single peak is observed at the expected position as predicted from the Fermi surface maximum cross-section area $S_{BZ}/S_k = 21.174$ perpendicular to $\vec{B}^{\,\mathrm{eff}}$.

Weak CDW ($V = 0.16$, $\mu = -0.2$): In this case, the Fermi surface is just slightly modified from the stacking of the model's two-dimensional Fermi surfaces and nearly cylindrically shaped, see right panel of Fig. 10. The periods of QOs are now dominated by both the maximum and the minimum Fermi surface cross-section areas perpendicular to $\vec{B}^{\,\mathrm{eff}}$. In particular, we calculate the QOs of the DOS over a range of $1/B \in [1000, 1400]$ on system size of length $L = 7.2 \times 10^5$, and the resulting Fourier transforms for the cases of $Q/B = 2$ and $Q/B = 20$ are shown in Fig. 12. A clear double peak structure is observed in both calculations. Again, the peak positions are consistent with the theory deduction from maximal and minimal Fermi surface cross section areas $S_{BZ}/S_k^{MAX} = 2.399$ and $S_{BZ}/S_k^{MIN} = 2.089$ for the $Q/B = 2$ case and $S_{BZ}/S_k^{MAX} = 2.2468$ and $S_{BZ}/S_k^{MIN} = 2.2226$ for the $Q/B = 20$ case, respectively.

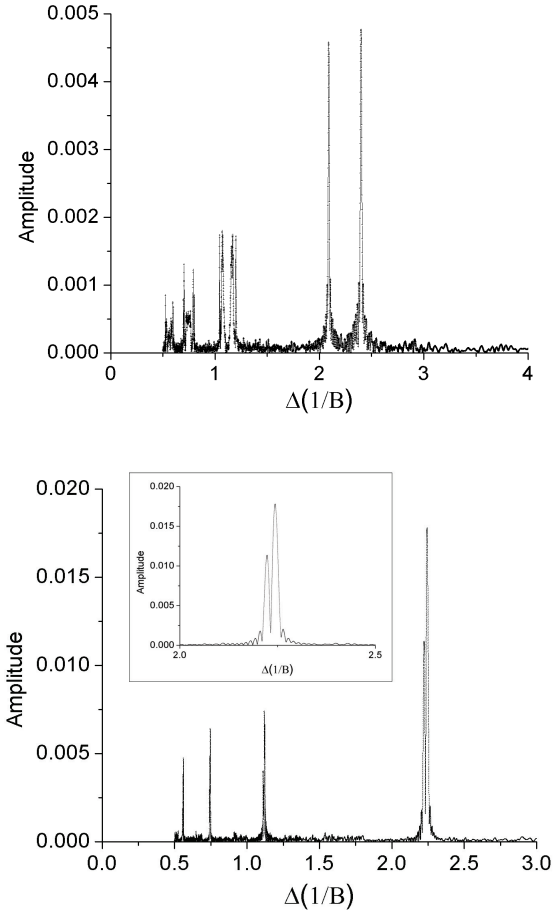

FIG. 12. Fourier transformations of the QOs of the DOS ρ for a weak CDW $V = 0.16$ and $\mu = -0.2$ over a range of $1/B \in [1000, 1400]$. A clear double-peak structure is observed. Upper panel: $Q/B = 2$, the peaks are at 2.089 and 2.399 as well as their higher harmonics; Lower panel: $Q/B = 20$, the peaks are at 2.2233 and 2.239 as well as their higher harmonics. The inset is an enlargement over the range of the double peaks. The system size is $L = 7.2 \times 10^5$.

B. Results

In the physical case, Q is generally expected to be approximately independent of magnetic field. (Although note that there are cases, such as the famous field-induced SDW states in $(TMTSF)_2ClO_4$, in which Q is strongly B dependent.[15]) In this case, both the magnitude and direction of $\vec{B}^{\,\text{eff}}$ varies as a function of B. In terms of the three-dimensional semiclassical trajectories, this means that the orientation of the orbits, and hence extremal cross-section areas $S_k^\perp(B)$, vary as a function of the applied magnetic field B, in addition to its usual dependence on the band structure parameters t, V, and μ. Since we are typically most interested in the small B limit, the most important cases are those in which $B^{\,\text{eff}}$ is only tilted slightly away from the $\hat{y}$ directions, and hence the semiclassical orbits lie close to the $x - z$ plane. Maxima in the semiclassical DOS

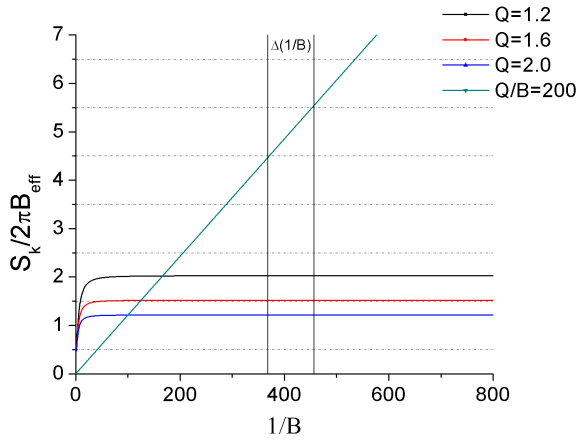

FIG. 13. The value of the orbital phase factor $S_k/2\pi B_{\,\text{eff}}$ over a range of magnetic field B: $1/B \in [0, 800]$ for a strong ICDWs with parameters $V = 1.6$, $\mu = -2.5$ and $Q = 1.2$ (black), $Q = 1.6$ (red), $Q = 2.0$ (blue), respectively. S_k is the maximal area of cross-sections perpendicular to $\vec{B}_{\,\text{eff}}$ for each given B. Results for fixed $Q/B = 200$ are also shown for comparison (cyan). Peaks in the DOS occur whenever these curves cross half-integer values, shown in the figures as the horizontal dashed lines.

are therefore found when

$$\frac{1}{\sqrt{B^2 + (Q/2\pi)^2}} = \left(n + \frac{1}{2}\right) \frac{2\pi}{S_k^\perp(B)} \tag{10}$$

From this equation it is clear that QOs which are perfectly periodic in $1/B$ are no longer possible for generic three-dimensional Fermi surfaces (i.e. generic cross-section areas $S_k^\perp(B)$). There is also a qualitative difference in the semiclassical trajectories for $V < V_c$, for which the Fermi surface forms a warped cylinder which is open in the $\hat{z}$ direction as shown in the right panel of Fig. 10, vs. $V > V_c$, in which case the Fermi surface is closed in the $\hat{z}$ direction, as shown in the left panel of the figure. Here $V_c(\mu)$ is the critical value of V at which a Lifshitz transition occurs at which the three-dimensional Fermi surface changes its topology.

1. *Absence of QOs for $V > V_c$*

So long as $V > V_c$, there is a well defined maximal cross-sectional area of Fermi surface contours perpendicular to $\hat{y}$. Moreover, for small B, the maximal cross-sectional area perpendicular to $\hat{B}^{\,\text{eff}}$, $S_k^\perp \lesssim S_{k,MAX}^\perp$, is close to and bounded by the maximum area for cross sections perpendicular to $\hat{y}$. Therefore, even if B is changed by an arbitrarily large factor, so long as $B \ll Q$, neither the magnitude of $\vec{B}^{\,\text{eff}}$, nor the value of $S_k^\perp$ changes substantially, and hence little variation is expected of the electronic structure. For example, we show in Fig. 13 the value $S_k/2\pi B_{\,\text{eff}}$ over a range of $1/B$ with parameters $V = 1.6$, $\mu = -2.5$ and $Q = 1.2$, 1.6, and 2.0. These curves do not intersect the half integers and are constrained to the quantum limit with only few Landau levels occupied for

reasonably small B, thus explaining the absence of QOs reported in Fig. 9. (The "ghost" of QOs in the $Q = 1.6$ case can be attributed to the fact that $S_k/2\pi B_{\rm eff}$ passes close to a half-integer value, where due to its vicinity to resonance the physical quantities are sensitive to small variation of the orbital phase factor). This can be contrasted with the case with a fixed $Q/B = 200$, where S_k is invariant and $S_k/2\pi B_{\rm eff}$ is linear in $B_{\rm eff}$, producing periodic QOs as a function of $1/B$.

Interestingly, for the same $V = 1.6$, $\mu = -2.5$ but a nearby commensurate CDW with $Q = \pi/2$, the model can be considered in the conventional framework of Sec. II B, and is a metal with one piece of closed Fermi surface. As expected, numerical calculations show clear and perfectly periodic QOs. Yet, we have shown that for a nearby incommensurate wave vector $Q = 1.6$ in Fig. 9, there are no well-defined QOs. We emphasize that treating the ICDW as an approximately commensurate CDW can be grossly misleading.

2. *Breakdown of semiclassical approximation for $V < V_c$*

For small values of V/W, the perturbative picture is useful. Nevertheless several new effects become apparent, even in this limit, when viewed from the dual perspective.

This is the regime where the three-dimensional Fermi surface is a warped cylinder as shown in the right panel of Fig. 10. The projections of the extremal three-dimensional Fermi surface cross sections $S_k^{\perp}(B)$ into the x-y plane, which we denote as $S_k^{\parallel}(B)$, is related to $S_k^{\perp}(B)$ by

$$S_k^{\parallel}(B) = \left(\frac{B}{B^{\rm eff}}\right) S_k^{\perp}(B), \tag{11}$$

and some typical projections are shown in Fig. 14. The "rippled" nature of the projected Fermi surface cross sections is a consequence of "neck and belly" variations along the $\hat{z}$ direction induced by the k_z dispersion in the effective three-dimensional Fermi surface; despite its complexity, the total area $S_k^{\parallel}(B)$ is close to that of the original two-dimensional Fermi surface in the absence of the CDW (red curves in Fig. 14), since the contributions from numerous "neck" and "belly" parts become averaged out. We therefore see that despite the absence of truly periodic oscillations in $1/B$, there exist approximately periodic oscillations since $S_k^{\perp}(B)/\sqrt{B^2 + (Q/2\pi)^2} = S_k^{\parallel}(B)/B \sim const/B$.

Nevertheless, since there are typically two or more extremal orbits of the three-dimensional Fermi surface, there are contributions from multiple $S_k^{\parallel}(B)$ and corresponding "fine structures" in the QOs. As an example, we show in Fig. 15 the QOs of both the localization length and the DOS with parameters $V = 0.16$, $\mu = -0.2$, $Q = 0.4$ over a range of relatively large magnetic field $1/B \in [80, 100]$. While the main QO period is clearly seen, there exist additional fine structures. As a consistency check, the red curves in Fig. 15 were obtained by summing over the contributions from all cross sections according to their respective semiclassical interference condition $S_k^{\parallel}(B)/B$.

As we move to smaller values of magnetic field B, $\vec{B}^{\rm eff}$ becomes closer to $\hat{y}$ and its perpendicular planes closer to the xz plane, thus the $S_k^{\perp}(B)$ cross sections span more Brillouin zones in the $\hat{z}$ direction. Inevitably, the extremal $S_k^{\parallel}(B)$ becomes closer and the fine structure gets suppressed. If we reduce B further, however, the projected Fermi surface becomes very complex and singular, as shown in the lower panel of Fig. 14. This is where the three-dimensional representation, while still exact, ceases to be useful due to a catastrophic magnetic breakdown of the semiclassical approximation.

Interestingly, there is a 'duality' between the magnetic breakdown scenarios in the original two-dimensional system and its dual three-dimensional model: the regime of the magnetic breakdown (QO period approximately determined by the

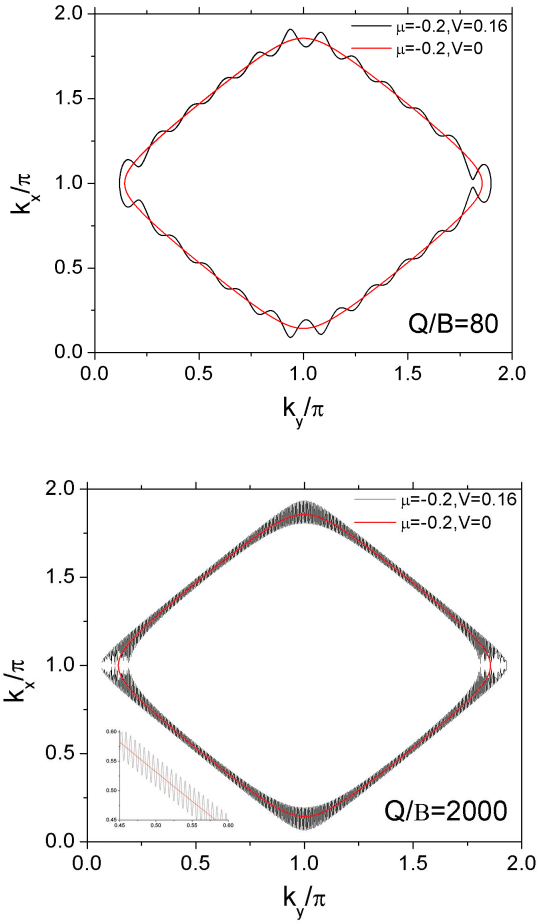

FIG. 14. The Fermi surfaces projected to the xy plane for parameters $V = 0.16$, $\mu = -0.2$ and $Q/B = 80$ (upper panel) and $Q/B = 2000$ (lower panel), respectively. The inset is an enlargement of a part of the Fermi surface. For comparison, the red curves show the original Fermi surface without the CDW.

Magnetic breakdown	Yes	No
Original 2D system	small Q/B and V	large Q/B and V
Dual 3D model	large Q/B and V	small Q/B and V

TABLE I. The duality between the magnetic breakdown parameter regimes of the original two-dimensional system and its dual three-dimensional version.

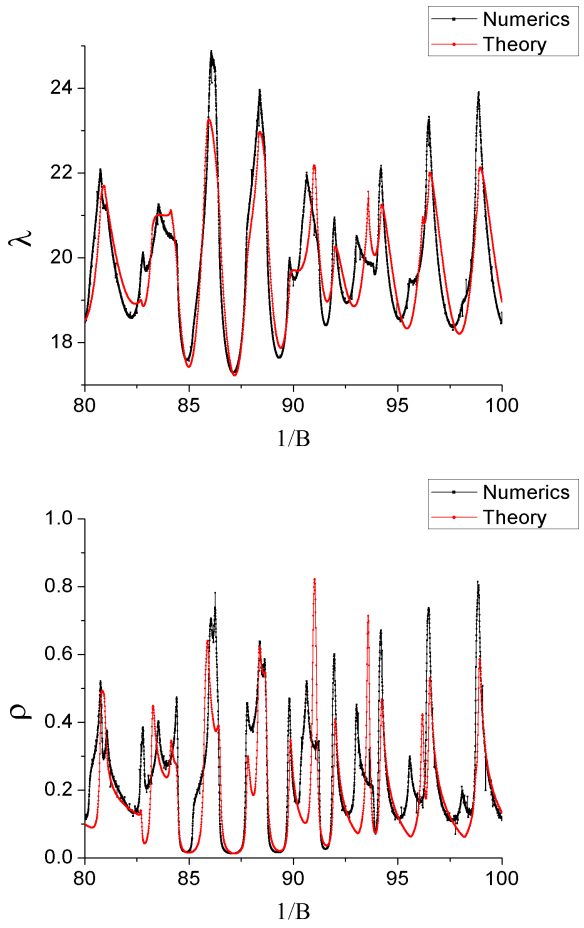

FIG. 15. The QOs of the localization length λ (upper panel) and DOS ρ (lower panel) as calculated numerically and compared with theoretical simulations over a range of relatively large magnetic field $1/B \in [80, 100]$ with parameters $V = 0.16$, $\mu = -0.2$, $Q = 0.4$. Additional fine structures and peaks are observed along with the fundamental oscillation period. The system size is $L = 7.2 \times 10^5$

Fermi surface without ICDW) in the original two-dimensional system corresponds in the dual three-dimensional model to the regime without magnetic breakdown; on the other hand, the two-dimensional reconstructed Fermi surface (without magnetic breakdown) is relevant when magnetic breakdown becomes important in the dual three-dimensional system. The qualitative results on the parameter regimes for the magnetic breakdowns in the dual scenarios are summarized in Table I. We discuss more details in Appendix B.

3. V_c is a crossover

While a sharp Lifshitz transition occurs in the three-dimensional band structure, this does not imply that there is a sharp transition in the QO spectrum at $V = V_c$. It is important to remember that for fixed Q, $|\vec{B}^{\text{eff}}| \geq Q$, so magnetic breakdown effects are significant wherever small gaps occur in the three-dimensional band structure. Of course, this situation necessarily arises as V approaches V_c. Consequently, in the exact solution, V_c marks a crossover in behavior – a crossover that is increasingly sharp as Q and B get smaller.

VI. GENERALIZATIONS OF THE DUALITY RELATIONS

A. Localization transition in an incommensurate potential

The problem of a one-dimensional chain in the presence of an ICDW is a classic problem that has been widely studied[10,11]. The corresponding eigenvalue equation is known as the "almost Mathieu equation." The dual mapping of this problem to a two-dimensional crystal in the presence of a magnetic field is equivalent to the Hofstadter problem with incommensurate flux density, $B = Q/2\pi$, and with hopping matrix elements 1 and $V/2$ along the $\hat{x}$ and $\hat{y}$ directions, respectively. (For $V = 2$, the one-dimensional equation is known as Harper's equation.)

This equation has been the subject of numerous studies focussing on the supposed "metal-insulator" transition which is thought to occur as a function of V; from delocalized states which occur for small V to purely localized states which occur for large V. In particular, it has been claimed[10,11] that for $V < 2$, all states are delocalized while for $V > 2$ all states are localized. We have found in our numerical solution of this problem as well as by analyzing the semiclassical dynamics in Hofstadter problem, that the former claim is likely incorrect - even for $V < 2$ states near the band bottom are localized so long as Q is truly irrational. We discuss this aspect of the problem in detail in a forthcoming paper,[16] but here we sketch the basic point.

In a magnetic field, the electron orbits in the two-dimensional momentum space are on the Fermi surface, which is given by the dispersion relation $\mu = \epsilon_k = 2\cos k_x + V\cos k_y$. Since the velocity of an electron at the Fermi energy is everywhere perpendicular to the Fermi surface, the semiclassical motion is localized in the $\hat{x}$ direction (which is the spatial direction in the original one-dimensional problem) unless the Fermi surface is open along the $\hat{y}$ direction. Thus, in the semiclassical approximation, for fixed μ, states at the Fermi level are delocalized provided $V \in (-2 + |\mu|, 2 - |\mu|)$, and otherwise are effectively localized. To test the validity of this semiclassical argument, we have numerically computed the Green's function $G(1, L)$ with the same parameters used to generate the two-dimensional Fermi surfaces in the upper panel of Fig. 16, assuming an incommensurate wave vector $Q = 1/31$; the results are shown in the lower panel of Fig. 16. Clearly, the semiclassical results are fully consistent with numerical calculations, in contradiction to claims that all states are delocalized for $V < 2$ (and $\mu \neq 0$).

It is important to remember that the CDW ordering vector Q plays the role of B^{eff} in this discussion. We have worked with a relatively small value of Q where the semiclassical results are expected to be more or less reliable, but for larger values of Q, magnetic breakdown should be exceedingly important, especially when V is smaller but close to the transition V_c. Therefore, for fixed $\mu \neq 0$, the critical value of V is shifted

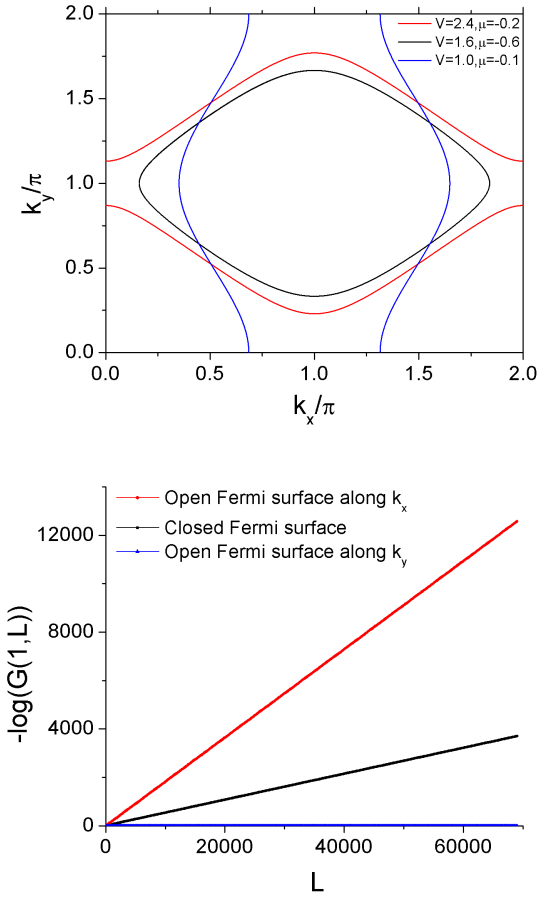

FIG. 16. The Fermi surfaces (upper panel) and the Green's function $-\log(G(1,L))$ versus L (lower panel) with parameters $V = 1.6$, $\mu = -0.6$ (black: closed Fermi surface), $V = 2.4$, $\mu = -0.2$ (red: open Fermi surface along the $\hat{x}$ direction) and $V = 1$, $\mu = -0.1$ (blue: open Fermi surface along the $\hat{y}$ direction), respectively. An exponential suppression is observed for the former two cases while the latter case indicates de-localization.

from the semiclassical value derived above. This effect has also been verified in our numerical calculations.

B. Bidirectional ICDW in a magnetic field

It is straightforward to generalize similar higher-dimensional dual models and lower-dimensional numerical methods to a bidirectional ICDW. For a d-dimensional hyper-cubic lattice in the presence of a uniform magnetic field and $H = \sum_{\vec{k}} H_{\vec{k}}$ with

$$
\begin{aligned}
H = &-\sum_{x,y,\vec{k}} t_x a^{\dagger}_{x+1,y,\vec{k}} a_{x,y,\vec{k}} + t_x a^{\dagger}_{x-1,y,\vec{k}} a_{x,y,\vec{k}} \\
&+ t_y e^{i\Phi_y x,\vec{k}} a^{\dagger}_{x,y+1,\vec{k}} a_{x,y,\vec{k}} + t_y e^{-i\Phi_y x} a^{\dagger}_{x,y-1,\vec{k}} a_{x,y,\vec{k}} + a^{\dagger}_{x,y,\vec{k}} a_{x,y,\vec{k}} \\
&\times \left[2\sum_{\nu=3}^{d} t_\nu \cos(\Phi_\nu x - k_\nu) + V_x \cos\left(Q_x x + k_z\right) + V_y \cos\left(Q_y y + k_w\right) \right]
\end{aligned}
\tag{12}
$$

where $\vec{k}$ is the Bloch vector for the $d-2$ dimensions other than the $\hat{x}$ and $\hat{y}$ directions. We have also denoted the initial phase of the CDW along the $\hat{x}$ and $\hat{y}$ directions as k_z and k_w, respectively.

Similar to the duality argument in Sec. III, by summing over both the k_z and k_w, the above system is equivalent to a $d+2$ dimensional effective model with two additional hoppings $V_x/2$ and $V_y/2$ along the $\hat{z}$ and $\hat{w}$ directions, and two additional magnetic fluxes Q_x through each xz plaquette, and Q_y through each yw plaquette, respectively. On the other hand, for efficient numerical calculations we can suppress the $\vec{k}$ indices and consider the resulting two-dimensional system. We leave more details to future work.

VII. CONCLUSIONS

For crystals - and this includes the case of a commensurate CDW – the existence of a sharp Fermi surface has the profound consequence that there exist exactly periodic oscillations in physical quantities as a function of $1/B$ in the limit $T \to 0$, $B \to 0$, and in the absence of disorder. In this precise sense, the breakdown of Bloch's theorem in the presence of an ICDW of arbitrary magnitude V eliminates the sharp definition of the Fermi surface and the exactly periodic character of the associated QOs. For small V, approximately periodic oscillations survive over parametrically broad ranges of B, but inevitably as B is reduced toward 0, the period of the oscillations shifts as smaller and smaller gaps opened in increasingly high order in perturbation theory become relevant. A crossover in the properties occurs at $V = V_c \sim W$, beyond which all periodic oscillations, and indeed essentially all magnetic field dependence of the electronic structure, is eliminated.

In real materials, disorder or finite temperature T limits the range of applicability of our results. At very low fields, when either T or the Dingle temperature T^* exceeds the cyclotron energy ω_c, all QOs are lost in a way that is independent of the nature of the CDW order.

We would like to thank Boris Spivak, Andre Broido, Danny Bulmash, Abhimanyu Banerjee, Yingfei Gu and Xiao-liang Qi for insightful discussions. This work is supported by the Stanford Institute for Theoretical Physics (YZ), the National Science Foundation through the grant No. DMR 1265593 (SAK) and DOE Office of Basic Energy Sciences under contract No. DEAC02-76SF00515(AM).

Appendix A: Green's function and recursive relations

Inspired by the recursive Green's function method, here we propose an efficient method to calculate some targeted Green's functions and their related physical measurable. First, it is straightforward to derive:

$$H_{ky} - \mu - i\delta = \begin{pmatrix} h_1 & 1 & & & \\ 1 & h_2 & 1 & & \\ & 1 & h_3 & 1 & \\ & & 1 & h_4 & \ddots \\ & & & \ddots & \ddots \end{pmatrix}$$

where $h_x = 2\cos\left(2\pi\Phi x + k_y\right) + V\cos\left(Qx + \phi\right) - \mu - i\delta$. Here δ denotes a very small imaginary part to round off the singularities and account for a finite line width for the energy levels and will be useful later in the Green's function. For large enough systems the detailed value of δ does not make essential changes to our results and conclusions. In particular, the Green's function for each k_y is given by the matrix inverse:

$$G_{k_y} = \left(\mu + i\delta - H_{k_y}\right)^{-1}$$

For simpler notation, let's define:

$$\mathcal{D}^i_j \equiv \det\begin{pmatrix} h_i & 1 & & & \\ 1 & h_{i+1} & 1 & & \\ & 1 & h_{i+2} & \ddots & \\ & & \ddots & \ddots & 1 \\ & & & 1 & h_j \end{pmatrix}$$

which has the following recursive relations:

$$\mathcal{D}^i_j = h_j\mathcal{D}^i_{j-1} - \mathcal{D}^i_{j-2}$$

$$\mathcal{D}^i_j = h_i\mathcal{D}^{i+1}_j - \mathcal{D}^{i+2}_j$$

or equivalently:

$$\mathcal{D}^i_j/\mathcal{D}^i_{j-1} = h_j - \mathcal{D}^i_{j-2}/\mathcal{D}^i_{j-1}$$

$$\mathcal{D}^i_j/\mathcal{D}^{i+1}_j = h_i - \mathcal{D}^{i+2}_j/\mathcal{D}^{i+1}_j$$

with the initial conditions: $\mathcal{D}^1_1 = h_1$, $\mathcal{D}^1_2 = h_1h_2 - 1$, $\mathcal{D}^L_L = h_L$ and $\mathcal{D}^{L-1}_L = h_{L-1}h_L - 1$.

The localization length:

The Green's function between two ends of the system along the $\hat{x}$ direction is exponentially suppressed as the system length L increases: $|G(1,L)| \sim \exp(-L/\lambda)$. λ is the localization length - an important property that characterizes transport behaviors of the system. To calculate $G(1,L)$ we need to trace over k_y:

$$G(1,L) = \sum_y G(\{1,y\};\{L,y\}) = \sum_{k_y} G_{k_y}(1,L)$$

yet we have shown in the main text that in the presence of a small magnetic field Φ, the localization length derived from $G(1,L)$ is equivalent to that from each individual $G_{k_y}(1,L)$.

Then, by standard matrix inversion procedure, it is not hard to obtain:

$$G_{k_y}(1,L) = (-1)^L/\mathcal{D}^1_L$$

which can be efficiently derived using the recursive relations. We can perform a log-linear fit with respect to L for the localization length λ.

Further, the above expression is consistent if we use $G(1,x) \sim \exp(-x/\lambda)$ to extract λ with a fixed system size L: $G_{k_y}(1,x) = (-1)^x\mathcal{D}^{x-1}_L/\mathcal{D}^1_L$.

The density of states(DOS):

The DOS at chemical potential μ is another important physical quantity that we mainly focus on:

$$\rho(\mu) = -\frac{1}{\pi LL_y}\sum_{x,k_y}\mathrm{Im}G_{k_y}(x,x) = -\frac{1}{\pi L}\sum_x \mathrm{Im}G_{k_y}(x,x)$$

Again, we have shown in the main text that the DOS averaged over k_y is equivalent to that for each specific k_y. We also note that:

$$\begin{aligned} &-G_{k_y}(x,x) = \mathcal{D}^1_{x-1}\mathcal{D}^{x+1}_L/\mathcal{D}^1_L \\ &= \mathcal{D}^1_{x-1}\mathcal{D}^{x+1}_L/\left(\mathcal{D}^1_{x-1}\mathcal{D}^{x+1}_L h_x - \mathcal{D}^1_{x-2}\mathcal{D}^{x+1}_L - \mathcal{D}^1_{x-1}\mathcal{D}^{x+2}_L + 2\right) \\ &\approx \left(h_x - \mathcal{D}^1_{x-2}/\mathcal{D}^1_{x-1} - \mathcal{D}^{x+2}_L/\mathcal{D}^{x+1}_L\right)^{-1} \end{aligned} \tag{A1}$$

where in the last step we have neglected the term of 2 since $2/\mathcal{D}^1_L$ is exponentially small. $-G_{k_y}(x,x)$ may be efficiently extracted with the recursive relations. Both λ and ρ should oscillate as a function of $1/B$ with periods given by the cross-section area of the Fermi surface.

Appendix B: Duality in magnetic breakdown scenarios

As we have shown in the main text, for $V \ll W$ and $B \ll Q$, the dual three-dimensional Fermi surface cross section's projected area onto the xy plane, $S^{\parallel}_k$, is almost invariant and asymptotically close to the original Fermi surface, therefore we expect QOs with a period $\Delta(1/B)$ in the regime where the electron semiclassical orbit restores the original Fermi surface. The magnetic breakdown in the original two-dimensional system are given by the dual three-dimensional model with no magnetic breakdown.

On the other hand, in the limit $B \to 0$, the magnetic breakdown in the original two-dimensional system gets washed out and the QOs are dominated by the CDW reconstructed Fermi surface. However, in this limit, the Fermi surface in the dual three-dimensional model also gets increasingly complex and singular (see Fig. 14 lower panel), and magnetic breakdown becomes essential. The electrons can tunnel between the ripples given $\ell\delta k > 1$ where ℓ is the magnetic length (that is almost constant since $B_{\text{eff}} \sim Q/2\pi$) and δk is the distance between two neighboring ripples, thus denser (larger Q/B) and

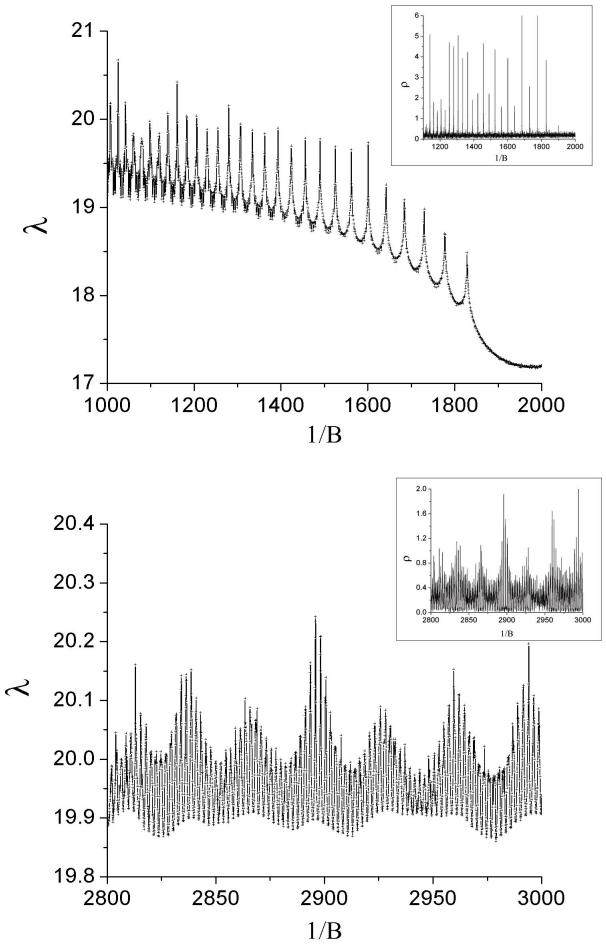

FIG. 17. Upper panel: The localization length λ and the DOS ρ (insets) with parameters $V = 0.16$, $\mu = -0.2$ and the ratio $Q/B = 2000$ fixed over a range of $1/B \in [1000, 2000]$ ($Q \in [1, 2]$). The oscillation becomes aperiodic and vanishes as B gets smaller. Lower panel: if we reduce B even further: $1/B \in [2800, 3000]$, the periodicity of the QO is well restored. The system size is $L = 7.2 \times 10^5$.

stronger (larger V) ripple structures are favorable to the magnetic breakdown, which is exactly opposite to the regimes of the original two-dimensional system, see Table I.

To manifest the impact of magnetic breakdown in the dual three-dimensional model, we present in Fig. 17 the numerical results on both the localization length and the DOS with a fixed ratio $Q/B = 2000$ for the Fermi surface in Fig. 14 lower panel. The resulting behaviors in the range $1/B \in [1000, 2000]$ are no longer periodic and essentially different from those in Fig. 12. This can be explained as the following: the magnetic breakdown introduces tunnelings between the ripples and effectively increases the area enclosed by the electron trajectory $S_k^{\parallel}(B)$. As we lower the magnetic field $B_{\text{eff}} \propto B$, the distance the electrons can tunnel through is reduced, thus $S_k^{\parallel}(B)$ is a decreasing function of $1/B$. When this happens, the orbital phase factor $S_k^{\parallel}(B)/B$ is slower than $1/B$, the periodicity in $1/B$ is lost and the interval between the oscillations becomes and larger, see Fig. 17 upper panel. On the other hand, when the magnetic field $B_{\text{eff}} \propto B$ is reduced further so that the magnetic breakdown becomes unimportant in the dual three-dimensional model, the periodicity should be restored. This is exactly what we observe in Fig. 17 lower panel.

[1] S. Chakravarty, Science, **319**, 735 (2008); S. Chakravarty, H-Y. Kee Proc. Natl. Acad. Sci. USA **105**, 8835 (2008)
[2] N. Doiron-Leyraud *et al.*, Nature **447**, 565-568 (2007).
[3] S. E. Sebastian et al., Phys. Rev. Lett. **108**, 196403 (2012).
[4] S. E. Sebastian et al., Nature **511**, 61-64 (2014).
[5] Andrea Allais, Debanjan Chowdhury, Subir Sachdev, arXiv-eprint:1406.0503.
[6] M. H. Cohen and L. M. Falikov, Phys. Rev. Lett. **7**, 231(1961).
[7] E. I. Blount, Phys. Rev. Lett. **4**, 114(1960).
[8] Jean-Michel Carter, Daniel Podolsky, and Hae-Young Kee, Phys. Rev. B **81**, 064519(2010).
[9] R. G. Chambers, Proc. Phys. Soc. London **88**, 701(1966).
[10] S. Aubry and C. André, Proc. Israel Physical Society, ed. C.G. Kuper 3 (Adam Hilger, Bristol, 1979) p. 133.
[11] J. B. Sokoloff, Physics Reports **126** No. 4, 189(1985).
[12] A. J. Millis and M. R. Norman, Phys. Rev. B **76**, 220503 (2007).
[13] H. Yao, D-H. Lee, and S. A. Kivelson, Phys. Rev. B **84**, 012507 (2011).
[14] Jonghyoun Eun, Zhiqiang Wang, and S. Chakravarty, Proc. Natl. Acad. Sci. **109**, 13198-13203 (2012).
[15] P.M. Chaikin, Journ. de Phys. I **6** , 1875-1898 (1996).
[16] Yi Zhang, Danny Bulmash, Akash V. Maharaj, Chao-ming Jian, and Steven A. Kivelson, to appear soon.
[17] Harper's equation is a specific realization of the almost Mathieu equation, with $t_y = t_x$.
[18] The origin of the higher harmonics can be attributed to non-linear dependence of the physical quantities on the orbital phase factor.